CMG-Augmented Control of a Hovering VTOL Platform

K. B. Lim*and D. D. Moerder†

Abstract

This paper describes how Control Moment Gyroscopes (CMGs) can be used for stability augmentation to a thrust vectoring system for a generic Vertical Take-Off and Landing platform. The response characteristics of the platform which uses only thrust vectoring and a second configuration which includes a single-gimbal CMG array are simulated and compared for hovering flight while subject to severe air turbulence. Simulation results demonstrate the effectiveness of a CMG array in its ability to significantly reduce the agility requirement on the thrust vectoring system. Albeit simplifying physical assumptions on a generic CMG configuration, the numerical results also suggest that reasonably sized CMGs will likely be sufficient for a small hovering vehicle.

1 Introduction

A Control Moment Gyroscope (CMG) array is a system that exerts transient torques for the purpose of control. Each CMG in the array consists of a spinning flywheel mounted in a frame, or gimbal, that can rotate normal to the flywheel's spin axis. This gimbal, in turn, is rigidly mounted to the system being controlled. The CMG exerts a torque on its attachment point by rotating the gimbal: The torque is the cross product of the flywheel angular momentum vector with that vector's rate of rotation; the latter is provided primarily by the gimbal rotation.

This paper considers using an array of single-axis-gimballed CMGs to control a small hovering Vertical Take-Off and Landing (VTOL) atmospheric flight vehicle with a thrust vectoring (TV) system. In this study, we subject the vehicle to a substantial level of disturbance from turbulent ambient air. Preserving tight control of attitude in the presence of heavy turbulence motivates using CMGs to augment the vehicle's aerodynamic control effectors, and this paper explores the impact of such augmentation on the agility required of the aerodynamic controls, and on the system mass.

From the control designer's point of view, the physics of a CMG array pose two important considerations that are not encountered when employing aerodynamic-based control:

- Useful torque in a CMG is very transient. For a fixed flywheel angular momentum, the torque magnitude is proportional to the gimbal rate of rotation; however, a rapidly rotating gimbal not only produces a large torque vector but rotates it rapidly.

*Senior Aerospace Technologist, Dynamic Systems & Controls Branch, kyong.b.lim@nasa.gov
†Senior Aerospace Technologist, Dynamic Systems & Controls Branch, d.d.moerder@larc.nasa.gov

- Because the CMG operates internally upon the airframe, rather than externally, upon the environment, there is no net change in vehicle angular momentum. If the CMG action imparts a particular angular momentum vector to the airframe, its negative is stored in the CMG array. If there is a sufficiently extended bias in the torque command realized by the CMG array, all of the gimbal mobility will ultimately be taken up in storing angular momentum. In order to avoid this loss of control, the airframe/CMG system must be desaturated by applying an external torque.

While the above considerations would seem to warn the potential aeronautical user away from CMGs, this paper will provide data that suggest that their use can be highly beneficial. Reverting to the two concerns above, consider:

- Although a CMG array cannot provide the sort of sustained torque needed for very low-frequency tasks, such as trim, it is very well-suited for control tasks involving higher frequencies. First, a substantial amount of angular momentum can be stored in even a small flywheel by spinning it rapidly – where small is meant relative to the airframe mass. When the gimbal is rotated at even modest speeds, large gyroscopic torques are produced, and these grow linearly with gimbal rate. Only modest actuation hardware is needed to generate abundant high-frequency control torques.
- Although the CMGs must be desaturated and, thus, require the presence of a control effector that can apply an external torque on the airframe, this externally applied desaturation need not be particularly agile. This relaxation of requirements on the vehicle's aerodynamic control performance can be used to specify lighter and/or cheaper control effectors, or to open up the vehicle design to using aerodynamic control technologies in which the effectors may have desirable properties, but be incapable of sufficient bandwidth to control the vehicle by themselves.

The vehicle considered in this paper is a small VTOL vehicle that uses TV for trim and control. This vehicle is very similar to one previously treated by the authors, in which a non-gimballed flywheel provided attitude stiffness via an angular momentum bias [1]. In [2], a Lyapunov-based nonlinear control scheme for CMG-based control of the same vehicle was reported. This study combined airframe and CMG states in a common control law, which stabilized the vehicle, but was difficult to tune. The authors examined disturbance rejection control of a fixed wing aircraft using conventional aerodynamic control along with the CMGs [3]. The flight controller assigned higher-frequency control activity to the CMGs, while slower control activity was realized by the aerodynamic control.

While this paper is a continuation of the work reported in [3], the vehicle size, aerodynamics, and flight condition are completely different from the earlier study. The vehicle is much lighter and smaller and hence more sensitive to air and payload disturbances. A more conventional control law [4] is considered for transparency. In the sequel, the controller structure outlined in [3] is applied to the vehicle for a parametric family of CMG arrays, indexed on the percentage of the total vehicle mass that they consume. It will be seen that even for a very modest expenditure of mass for supplying the vehicle with a CMG system, the required bandwidth of the vectored thrust system can be dramatically reduced, and the vehicle's attitude hold performance dramatically improved in heavy turbulence. The steering law algorithm includes logic to detect proximity to singularities, and then transfers the torque command components in the most uncontrollable subspace to the

thrust vectoring system. It will be seen, however, that such singularities did not occur in the cases considered; hence we defer a detailed description of this logic to a future paper.

2 Dynamics and Control of Hovering Platform

Figure 1 shows a sketch of the vehicle and key nominal parameters for the vehicle, CMG array, and quad ducted fan considered in this study. It is a small square platform with a shrouded propeller

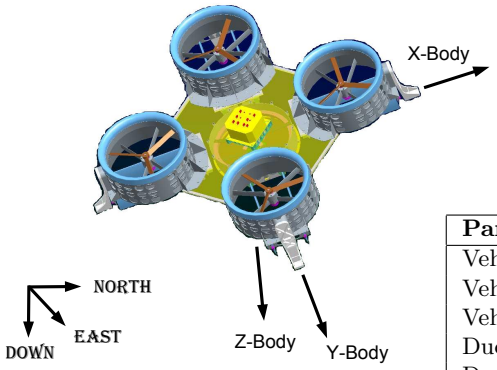

Parameter	Symbol	Value	Units
Vehicle mass (including CMGs)	m	20	kg
Vehicle length,width, height	l_1, l_2, l_3	.9, .9, .3	m
Vehicle second moment of inertia	I_1, I_2, I_3	.59, .58, 1.15	kgm^2
Ducted fan rotor inertia (each)	I_F^a	.002	kgm^2
Ducted fan speed (range)	ω_s	5 to 12	krpm
Ducted fan control vane (range)	θ_{vane}	-30 to 30	deg
CMG wheel mass (each)	m_c	.05 to .5	kg
CMG wheel diameter	d_c	.152	m
CMG wheel speed	Ω	31,354	rpm
CMG angular momenta (each)	H_W	.951 to 9.51	Nms
CMG gimbal axis tilt angle	θ_o	54	deg

Figure 1: Schematic of a generic quad ducted fan, CMG-assisted flying platform.

at each corner. The vehicle's body axes have their origin at the center of mass, and are oriented as shown in Figure 2, with the z-body axis pointed into the page. Thrust vectoring vanes are mounted downstream of each propeller, and each set of vanes diverts the thrust along the body axis normal to the body axis that passes through the thruster. The Figure displays both the vehicle body axes and four local coordinate systems for the four thrusters: $F_{F_j}, \quad j = 1, 2, 3, 4$. The thrust deflections due to thrust vectoring vanes are parallel to the y axes of the F_{F_j} frames. The CMG unit is assumed to be rigidly attached to the vehicle which, itself, is assumed rigid.

The closed-loop simulation simplifies the actuation dynamics as follows. The electric motors driving the propellers are modelled with linear first-order transfer functions, and the servos for the TV vanes with second-order ones. The parameter values for these dynamics are varied in the study for various CMG cases, and are detailed in the next section. The CMG flywheels are assumed to spin with constant speed, and the dynamics of the motors driving their gimbals are ignored. Each gimbal's motion commands are implemented with a servo loop having 20-Hz bandwidth. It should be noted that the TV transfer functions appear only in the simulation, and are not used in the control design.

Although the simulation model of the vehicle fully couples the dynamics of the airframe/propulsion

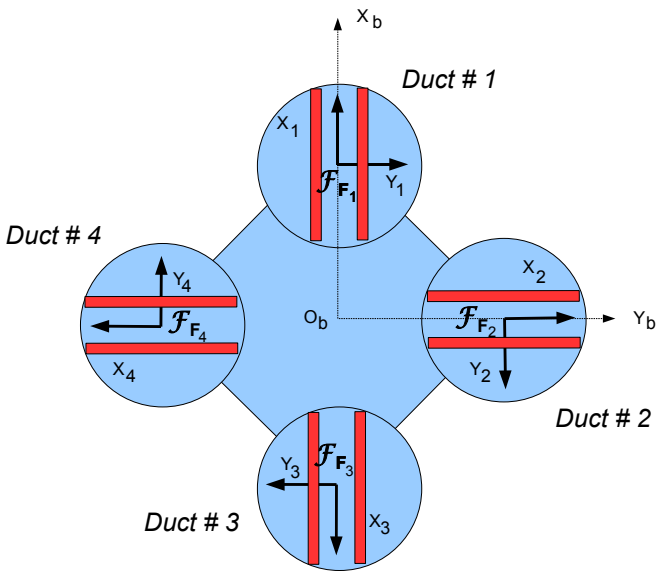

Figure 2: Top view of ducted fan frame orientations relative to platform body frame.

system to those of the CMG array, they are separated in the control design, continuing the approach taken in [3]. The CMG appears in the airframe control law only as a torque source, and is internally controlled by a steering law. The vehicle control law regulates the velocity, $v \in \mathcal{R}^{3\times 1}$, of the center of mass, and its attitude and angular velocity, $\omega \in \mathcal{R}^{3\times 1}$. The vehicle attitude is represented by its four-element vector of Euler parameters, $e^T = [e_0, e_1, e_2, e_3]$, so that

$$\dot{e} = \frac{1}{2}[e] \begin{bmatrix} 0 \\ \omega \end{bmatrix}, \qquad \|e\| = 1 \tag{1}$$

where

$$[e] = \begin{bmatrix} e_0 & -e_1 & -e_2 & -e_3 \\ e_1 & e_0 & -e_3 & e_2 \\ e_2 & e_3 & e_0 & -e_1 \\ e_3 & -e_2 & e_1 & e_0 \end{bmatrix} \tag{2}$$

The vehicle control structure separates control forces, $u_v \in \mathcal{R}^{3\times 1}$, and torques, $u_\tau \in \mathcal{R}^{3\times 1}$, to regulate v, ω, e. For hovering, the control forces are designed to satisfy

$$u_v + mC_{bo}g_o - m\omega^{\times}v - mf_{\text{aero}} = G_v v \tag{3}$$

where $C_{bo} \in \mathcal{R}^{3\times 3}$ transforms the North-East-Down (NED) frame gravity g_o to body axes, m is vehicle mass, f_{aero} is aerodynamic force on the airframe, $G_v \in \mathcal{R}^{3\times 3}$ is a gain matrix for velocity tracking error, and the $(\cdot)^{\times}$ notation denotes the skew symmetric matrix associated with the cross product, for example

$$\omega^{\times} = \begin{bmatrix} 0 & -\omega_3 & \omega_2 \\ \omega_3 & 0 & -\omega_1 \\ -\omega_2 & \omega_1 & 0 \end{bmatrix} \tag{4}$$

The control law for the rotational dynamics is

$$u_\tau - \tau_{\text{aero}} = k_\omega \omega - k_\epsilon \tilde{\epsilon} \tag{5}$$

where τ_{aero} is the set of aerodynamic torques operating on the airframe, $k_\omega \in \mathcal{R}^{3\times 3}$ and $k_\epsilon \in \mathcal{R}^{3\times 3}$ denote gain matrices on the angular velocity and attitude tracking errors, and $\tilde{\epsilon}^T = [\epsilon_1, \epsilon_2, \epsilon_3]$ is a portion of the attitude deviation vector ϵ about a desired target trim attitude $\bar{e}$ where

$$\begin{Bmatrix} \epsilon_0 \\ \epsilon_1 \\ \epsilon_2 \\ \epsilon_3 \end{Bmatrix} = \begin{bmatrix} e_0 & e_1 & e_2 & -e_3 \\ e_1 & -e_0 & -e_3 & e_2 \\ e_2 & e_3 & -e_0 & -e_1 \\ e_3 & -e_2 & e_1 & -e_0 \end{bmatrix} \begin{Bmatrix} \bar{e}_0 \\ \bar{e}_1 \\ \bar{e}_2 \\ \bar{e}_3 \end{Bmatrix} \tag{6}$$

denotes the sequential rotational relationships for Euler parameters (see for example [6]). All subsequent simulation results shown in this paper are based on the above simple control structure. Other, more complicated, approaches were tried and, when applied by the authors, gave very similar results for the hovering disturbance rejection problem. These included (1) a nonlinear feedback version of equation 5 as given in [4], (2) a nonlinear quaternion feedback described in [7] and [8], and (3) a linear feedback on the attitude excursions of the vehicle about a target attitude as measured by Modified Rodrigues parameters, as proposed in [9].

The control forces, u_v are generated entirely by the TV system; on the other hand, the control torques can be separated as

$$u_\tau = u_{\text{ext}} + u_{\text{int}} \tag{7}$$

where u_{ext} is external torque coming from the TV system and u_{int} is internal torque due to the CMG. Recall, from the introduction, that the CMG system most advantageously generates high-frequency torques. The TV system, on the other hand, is the only effector capable of steady torques, and most easily produces low-frequency ones. This motivates splitting u_τ on the basis of frequency bands assigned to u_{ext} and u_{int} (as in [3]), done by high-pass filtering u_τ to give u_τ^h, and

$$\left.\begin{array}{rcll} u_{\text{int}} & = & u_\tau^h & \text{assigned to CMG} \\ u_{\text{ext}} & = & u_\tau - u_{\text{int}} & \text{assigned to TV} \end{array}\right\} \tag{8}$$

The thrust vectoring system has eight degrees of control freedom available, and these are allocated to the airframe rigid body dynamics via the following weighted least squares algorithm,

$$\begin{bmatrix} \delta\omega_{_F} \\ \delta\theta_{_F} \end{bmatrix} = W_F^{-1} \left(J_F W_F^{-1}\right)^+ \begin{bmatrix} \delta u_v \\ \delta u_{\text{ext}} \end{bmatrix} \tag{9}$$

where $(\cdot)^+$ denotes pseudo-inverse and the change in TV commands about hovering trim are

$$\left.\begin{array}{rcll} \delta\omega_{_F}^T & = & \left[\delta\omega_{_{F_1}}, \delta\omega_{_{F_2}}, \delta\omega_{_{F_3}}, \delta\omega_{_{F_4}}\right] & \text{propeller speed commands} \\ \delta\theta_{_F}^T & = & \left[\delta\theta_{_{F_1}}, \delta\theta_{_{F_2}}, \delta\theta_{_{F_3}}, \delta\theta_{_{F_4}}\right] & \text{vane commands} \end{array}\right\} \tag{10}$$

where W_F is a weighting matrix, and where the Jacobian matrix J_F evaluated at hovering trim condiditon is

$$J_F = \left[\begin{array}{cc} \partial u_v/\partial\omega_{_F} & \partial u_v/\partial\theta_{_F} \\ \partial u_{\text{ext}}/\partial\omega_{_F} & \partial u_{\text{ext}}/\partial\theta_{_F} \end{array}\right]_{trim} \tag{11}$$

The internal torque equations for the vehicle and CMG can be solved for the gimbal rates $\dot{\eta}^T = [\dot{\eta_1}, \dot{\eta_2}, \dot{\eta_3}, \dot{\eta_4}]$ that result in the desired u_{int}. The equations are affine in $\dot{\eta}$, so that the internal torque can be expressed as

$$C(\eta, \omega)\dot{\eta} = -u_{\text{int}} - \psi(\eta, \ddot{\eta}, \omega) \tag{12}$$

where the nonlinear terms have been gathered into $C \in \mathcal{R}^{3\times 4}$ and ψ, and is solved for $\dot{\eta}$ via pseudoinverse.

3 Simulation of Hovering Vehicle Subject to Turbulence

In the following simulations, four different CMG systems are considered which differ only in their masses which range from 10% of vehicle (Case 2-1) to 1% of vehicle (Case 2-4). For the sake of simplicity, we assume that the diameter of each CMG wheel is fixed at 6 inches and its tip velocity fixed at 250 meters per second, which is considered a high, but achievable, rate for steel flywheels. With these assumptions, each wheel is assumed to be spinning at the constant speed of $31,354$ rpm.

3.1 Simulation Conditions

The following Table 1 shows the vehicle control effector configurations and associated parameters considered during hovering and subjected to severe air turbulence. Cases 1-1 and 1-2 are TV-only

Case	**Control Effector**	**Bandwidth of TV** (Hz)	**Attitude Gain** $k_\epsilon/100$	**HP Filter** $(\omega_{_{HP}}, Hz)$
1-1	Thrust Vectoring	2.00	$diag(1,1,2)$	-
1-2	Thrust Vectoring	10.00	$diag(1,2,5)$	-
2-1	with CMG @ 10 % of Vehicle mass	0.20	$diag(1,2,5)$	.10
2-2	with CMG @ 5 % of Vehicle mass	0.75	$diag(1,2,5)$	.15
2-3	with CMG @ 2 % of Vehicle mass	1.75	$diag(1,2,5)$	.25
2-4	with CMG @ 1 % of Vehicle mass	2.00	$diag(1,2,5)$	.50

Table 1: Control effector configurations considered.

cases while the remaining four include CMG augmentation with different masses. The column denoting the bandwidth of TV refers to the tracking bandwidth of the control vane and fan speed commands in the thrust vectoring system. In all the cases, these TV dynamics neglected during the control design phase, but included in the closed loop simulation results shown. Case 1-1 assumes TV only with a bandwidth of 2 Hz while Case 1-2 assumes an increased bandwidth of 10 Hz. The remaining four cases which are CMG-augmented assumes gradually increasing TV bandwidths of up to 2 Hz. Notice from the above table that for the CMGs, the two key parameters of interest in this study are its relative mass to the vehicle and the high-pass filter break frequency for torque allocation. The basic idea for the above choice of control effector configurations considered are (a) to use Cases 1-1 and 1-2 as baselines for comparisons, and (b) to illustrate the lower values of torque frequencies that can be allocated to CMGs if their weights (and correspondingly their angular momentum capacities) increase.

The TV control bandwidth of the existing laboratory ducted fans and vanes is approximately 2 Hertz. The intent in considering a fictitious bandwidth of 10 Hertz for the TV control system are to (a) investigate the vehicle performance *if* there exists a more agile ideal TV system and (b) to serve as a baseline when the CMG augmented cases are analyzed. For practical reasons, it is important to note that the effects of transient aerodynamics at higher bandwidths may be unknown or at best difficult to predict. Physical intuition suggests that uncertainties in the time histories of the net forces and moments acting on the vehicle will likely increase with an increasing control bandwidth of a fluidic-based TV system.

The control law given in equations 3 and 5 are used to generate commands for translational and attitude control in all six cases. While the same angular velocity error gains of

$$k_\omega = 20 I_{3\times 3} \tag{13}$$

are assumed in all cases, the attitude error gains are slightly different as given in the Table 1. Naturally, larger gains would lead to superior attitude response provided that the control system can deliver with sufficient fidelity the commanded forces and torques in view of saturation and rate limits. In all cases, the following velocity regulation gains are used while hovering:

$$G_v = -0.2 I_{3\times 3} \tag{14}$$

For torque allocation between TV and CMGs, a second order high-pass filter with the break frequencies listed in Table 1 are assumed.

A single simulated wind time history based on "severe" Dryden turbulence spectra, based on NED frame, are used in all simulations. These winds are assumed to act on the vehicle for the first 50 seconds followed by 10 seconds of free transient response.

3.2 Response to Severe Turbulence

Figures 3 show the time history of the gust velocity relative to ground whose components are expressed in NED frame for Case 1-1. These "severe" turbulence are assumed to act in the first 50 seconds and results in the airspeed and aerodynamic angles. Notice the erratic AOA and sideslip angles due to the continuous turbulence. These wind states are similar for all the remaining cases and are not shown.

Figure 4 shows the resulting aerodynamic force and moment loads on vehicle for Case 1-1. The aerodynamic vehicle loads for the remaining cases are similar and are not shown. Notice that the aerodynamic force loads on the vehicle in the longitudinal plane easily exceeds half gs (about 98 N) whereas the side forces are significantly less. The aerodynamic moment loads appear to be about the same magnitude in all three axes although Pitch moments appear the largest. The power spectral densities for these loads show the characteristic rolloff in a Dryden spectrum model [5].

Figure 5 shows the vehicle attitude response with respect to the NED frame due to severe air turbulence while hovering. The attitude response for Case 1-1 is clearly the worst while the other TV only Case 1-2 gave very similar response to the remaining four CMG-augmented responses (Cases 2-1 to 2-4). However, notice the erratic Yaw response for Case 1-2 at about 50 seconds into the simulation, a sign of degraded stability. During the attitude error gain design, for all six cases, the Yaw-angle excursions were disproportionately large so that the attitude gains for Yaw angles were increased in an attempt to mitigate the Yaw angle response. These gains were increased as much as possible without destabilizing the vehicle, and resulted in the gains as given in Table 1. Although the four CMG-augmented cases allowed the largest increase in this gain to produce the smallest Yaw-angle response, the same gains as used in Case 1-2 were selected, for comparison purposes. On the other hand, the larger Yaw response as shown for TV-only Case 1-1 could not be further attenuated by changing its Yaw gains without destabilizing the vehicle.

Figure 6 shows the ground velocity component in the NED frame response to severe air turbulence while hovering for Cases 1-1 and 1-2. The remaining CMG-augmented cases gives similar ground velocity responses as in Case 1-2. In each case, the vehicle picks up a non-negligible level of ground speed in the Forward and and Down directions but with the end of turbulence, tries to recover a hovering state. Case 1-1 appears to give slightly larger responses than the remaining cases.

Figure 7 shows vehicle angular velocity component responses to severe air turbulence while hovering. This angular velocity response confirms the earlier notion that Cases 2-1 to 2-4 gives improved attitude regulation performance over Cases 1-1 and 1-2. Interestingly, under light winds (not shown here for brevity), there were no significant diferences in the attitude regulation performance.

Figure 8 shows the commanded (dotted line) and actual (solid line) control forces and Figure 9 shows the corresponding torques generated by the ducted fan in response to severe turbulence while hovering. Observe the following:

- The trends (or slowly time-varying component of the signal) in both the commanded and realized control forces and moments from the ducted fan are similar in all cases. This is not unexpected since the same disturbances and control laws were used for all cases.
- Higher frequency ducted fan force components are noticably absent in all cases including the TV only cases. However, large amplitude higher frequency ducted fan moment components are evident for Cases 1-1 and 1-2, and noticeably absent for CMG-augmented cases, Cases 2-1 to 2-4. Clearly, the CMGs alleviated the burden on the thrust vectoring ducted fan system by transferring higher frequency commanded torque components to the CMGs.
- In all cases, there are significant tracking errors in the commanded ducted fan forces and moments. However, the commanded forces in the Body 3-axis are tracked relatively well in all cases because the ducted fans are collinear to this Body axis and hence a collective change in fan speeds can readily generate forces along this axis. By the same token, the commanded

forces orthogonal to this axis are not tracked well as seen by the large tracking error in the Body 1-axis, which evidently produces a larger ground velocity error component in the North direction. The commanded forces in the Body 2-axis is tracked relatively well partly because the commanded magnitudes are smaller, due to the smaller aerodynamic disturbances in this lateral direction.

- Relatively large errors in the commanded Yaw axis torque are seen. These are mostly slowly time-varying but contain some higher-frequency content for Case 1-1 and 1-2 whose Yaw attitude excursions are relatively large at corresponding periods. This particular response appears consistent with the fact that commanded Roll and Pitch torques can be generated readily via differential thrusting while the Yaw torques are mostly the result of collective vane deflections, and is more limted as seen by the prevalence of vane saturations unlike the fan speeds that did not saturate, as shown in the figures to follow.

Figures 10 and 11 show respectively the ducted fan speeds and control vane angle deflections that generated the control forces and moments shown earlier. Observe the following:

- The ducted fan speed and vane deflection responses for TV-only cases (Cases 1-1 and 1-2) are significantly more active than CMG-augmented cases (Cases 2-1 to 2-4). This is because TV-only cases must generate all commanded forces and torques at all frequencies. Of course commanded forces are usually of lower frequency in nature due to mostly translational motion so that higher frequency torque commands for attitude control are the challenging requirement for TV-only cases.

- Among the CMG-augmented cases, note that more rapidly varying fan speeds and vanes are required going from Case 2-1 to Case 2-4. This is because the ducted fans must be increasingly more agile to take on higher frequency commands as the CMGs' momentum capacity decreases.

Figures 12 and 13 show the frequency composition in terms of the power spectral densities for each duct fan speed excursion from trim values and vane deflection angles. The CMG-augmented Cases 2-1 to 2-4 show significantly less higher frequency component in its ducted fan speed and control vane signals than either purely thrust vectoring Cases 1-1 and 1-2. The approximate frequency at which these two sets of responses starts to diverge is approximately 1 Hz, in the vicinity of the high-pass filter break frequency used.

Figure 14 shows the CMG reaction torque components on the CMG system (opposite of CMG torque acting on the vehicle) and the corresponding gimbal rates that produced it for all four cases. Figure 15 shows the gimbal motor torques and their comparisons to the CMG reaction torques produced. Notice the following:

- The CMG reaction torques produced by the larger CMG in Case 2-1 (having largest angular momentum) appears to be larger mostly because of the presence of more lower-frequency torques than the lighter CMG Case 2-4 (having least angular momentum). Of course, this is partly because one can allocate lower torque commands to the CMG case with higher angular momentum capacity. However, note that the higher frequency torque components are similar for all four cases, clearly a consequence of requiring attenuation of responses to the same higher frequency disturbances using CMGs.

- Lower gimbal rates are required for the heavier CMGs, for the same torque disturbances, because of their larger angular momentum. This also makes it easier for the heavier CMGs to generate lower frequency torque commands.
- The gimbal motor torques are significantly larger for larger mass CMG Case 2-1 than smaller mass Case 2-4 although Case 2-1 required smaller gimbal rates than Case 2-4. Considering a cursory accounting of the gimbal motor torque as an inertial effect consisting of the product of gimbal rotational inertia and the gimbal angle rotational accelerations, recall that the rotational inertia of Case 2-1 is ten times that of Case 2-4.

3.3 CMG responses while hovering under turbulences

Figure 16 shows a comparison of the standard deviation of the CMG associated responses for all four CMG cases. The heavier CMGs (Case 2-1, or Case Number 1) generate larger torques using slower gimbal rates (to generate lower frequency torques) but require larger gimbal motor torques. The lighter CMGs (case 2-4, or Case Number 4) appear to produce the largest mean torque amplification with the highest gimbal rates, but require the smallest gimbal motor torques.

3.4 Summary of Simulation Results

Figure 17 shows standard deviation comparisons of the vehicle attitude and thrust vectoring effector responses. Note that the main difference between the TV-only cases and CMG-augmented cases are in their rates of change in the attitude or control effectors.

At light turbulence levels during hovering it turns out that the benefits of CMG augmentation are not noticable. This conclusion is based on simulation results not shown in this paper for brevity. However, under severe turbulence, given a similar level of vehicle attitude and translational performance, the CMG-augmented cases required significantly less agile TV machinery. This apparently is the successful result of allocating higher frequency control torque components to the CMGs instead of the bandlimited shrouded propeller/vane units. With winds that have a large mean velocity component, however, the design of a torque allocation filter must be made carefully in order to avoid saturating the CMGs.

Figure 18 shows a dependence of the high-pass filter break frequency on the total mass of the CMGs used in this study. The CMGs with larger mass allow the generation of lower frequency control torques, significantly relaxing the requirement on the thrust vectoring agility.

4 Conclusions

This paper has examined the utility of including a CMG array in the control effector suite for a small hovering VTOL atmospheric flight vehicle with a TV system. The control scenario considered was attitude and translational velocity regulation in atmospheric turbulence. The study compared a parametric family of CMGs, indexed on mass, to determine whether a CMG array might "buy its way" into the system by providing a control benefit that justified its mass and complexity. It was seen that it certainly did not – at least when turbulence was very light; in that case, the system

was well-served by its TV system. If, on the other hand, the system was subjected to heavy Dryden turbulence, the vehicle could not be controlled, even when artifically increasing the thrust-vectoring bandwidth by a factor of five. Inclusion of even a tiny (1% of vehicle mass) CMG array permitted good stabilization with the nominal TV hardware bandwidth.

More intriguingly, increasing the size of the CMG array to 5% of vehicle mass allowed reducing the thrust vectoring hardware bandwidth by more than a factor of two. This suggests that the inclusion of a CMG array can allow substantial relaxation of the agility required of the vehicle's aerodynamic controls. This leads to a reduction in transient-aero-based modelling uncertainty, and also opens additional choices for the fluidic hardware to be used. Finally, it should be noted that the above conclusions are based on assumed simulated turbulence and vehicle aerodynamic models that are neither validated by experimental data nor modeled by CFD methods.

References

[1] Lim,K.B., Shin,J.Y., and Moerder, D.D., "Bias momentum sizing for hovering dual-spin platforms," NASA Technical Paper 2006-214317, NASA Langley Research Center, Hampton, Virginia, May 2006.

[2] Lim, K.B., Shin, J.Y., and Moerder, D.D., "Variable speed CMG control of a dual-spin stabilized unconventional VTOL air vehicle," AIAA 3rd *Unmanned Unlimited* Technical Conference, Workshop & Exhibit, September 20-23, 2004, Chicago, IL, AIAA Paper 2004-6537.

[3] Lim, K.B., and Moerder, D.D., "A feasibility study on the control of a generic air vehicle using control moment gyros," AIAA Guidance, Navigation, & Control Conference, August 21-24, 2006, Keystone, CO, AIAA Paper 2006-6313.

[4] Wie, B., and Barba, P.M., "Quaternion feedback for spacecraft large angle maneuvers", *Journal of Guidance, Control, and Dynamics*, Vol. 8, No. 3, 1985, pp. 360-5.

[5] Wie, Bong, *Gust Loads on Aircraft: Concepts and Applications*, AIAA Education Series, Reston, Virginia, 1988. Chapter 4.

[6] *Spacecraft attitude determination and control*, Ed. by James R. Wertz, Astrophysics and Space Science Library, vol. 73, Kluwer Academic Publishers, Boston, 1978, p. 416-.

[7] Wen, J.T., and Kreutz-Delgado, K., "The attitude control problem", *IEEE Transactions on Automatic Control*, vol. 36, no. 10, 1991, pp. 1148-1163.

[8] Joshi, S.M., Kelkar, A.G., and Wen, J.T.-Y., "Robust attitude stabilization of spacecraft using nonlinear quaternion feedback", *IEEE Transactions on Automatic Control*, vol. 40, no. 10, 1995, pp. 1800-3.

[9] Tsiotras, P., "New control laws for the attitude stabilization of rigid bodies," Proceedings of *IFAC symposium on Automatic Control in Aerospace*, Palo Alto, CA., Sept 12-16, 1994, pp. 316-321.

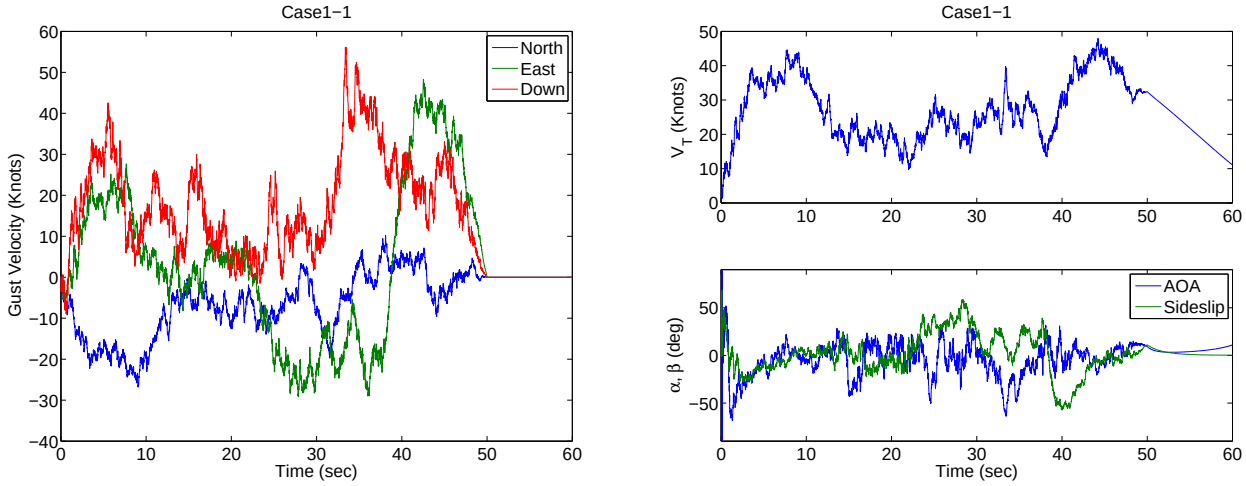

Figure 3: Gust velocity due to severe air turbulence while hovering and the resulting airspeed and aerodynamic angle response for Case 1-1.

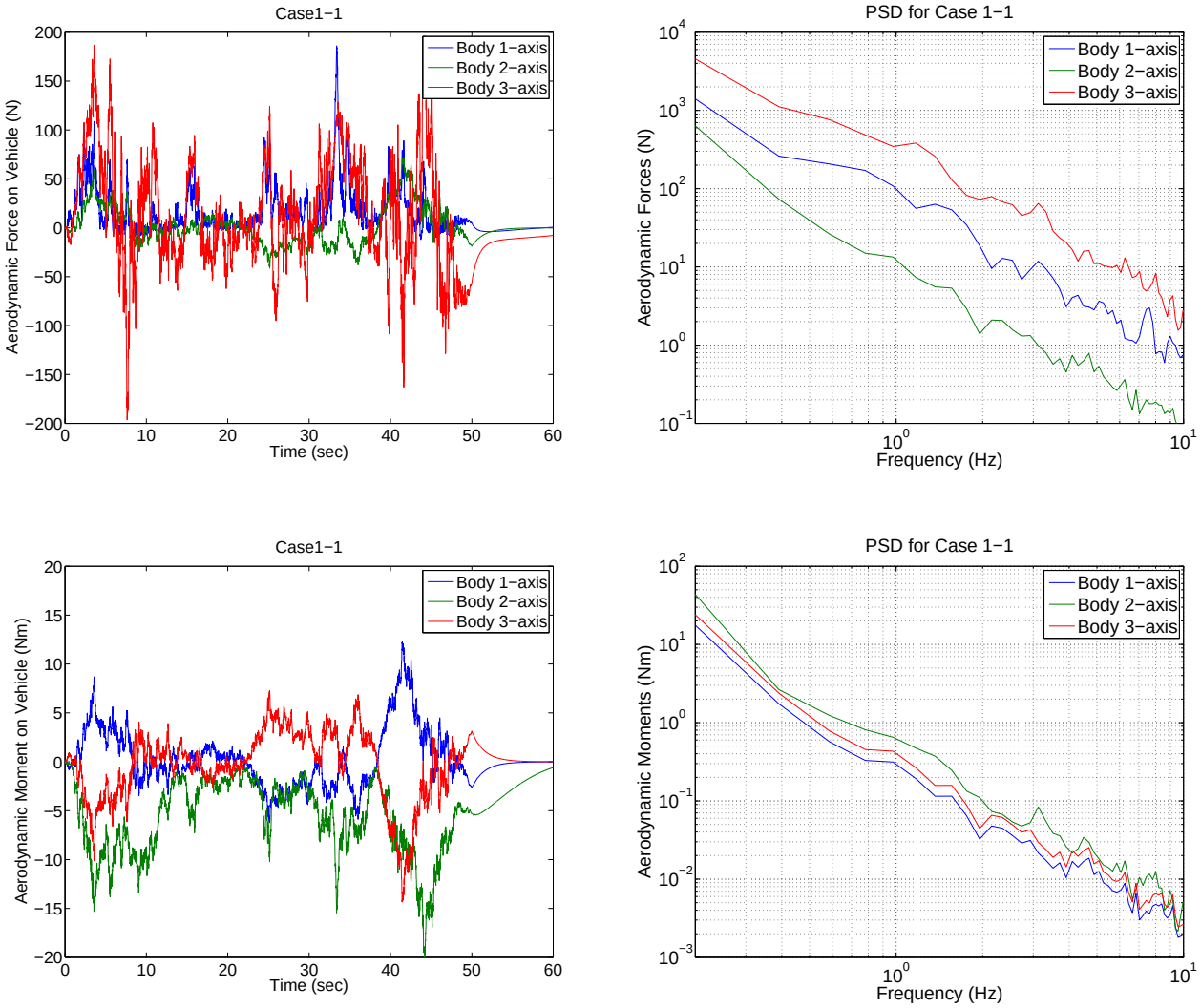

Figure 4: Aerodynamic loads on vehicle due to severe turbulence while hovering for Case 1-1.

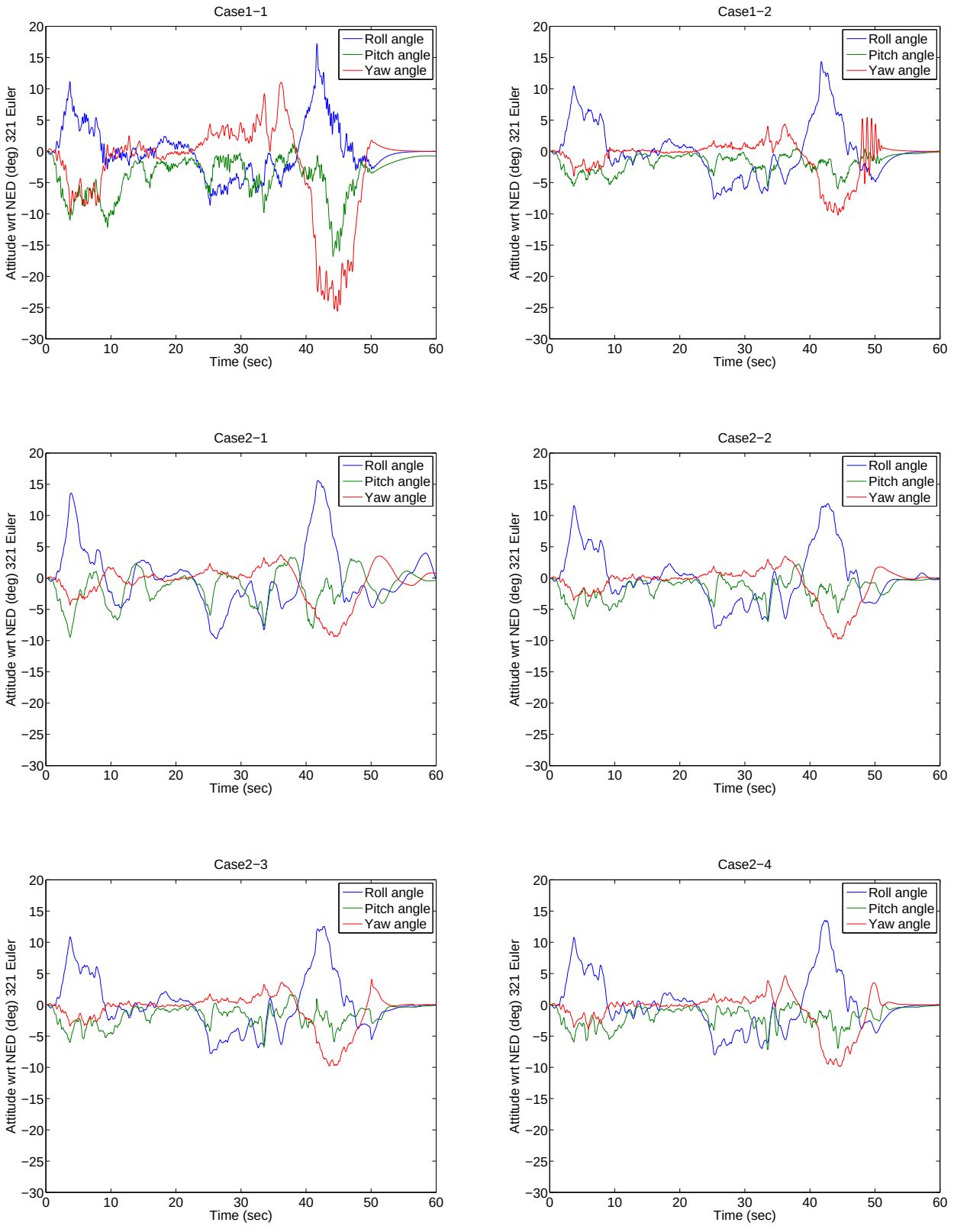

Figure 5: Attitude response to severe turbulence while hovering for Cases 1-1 and 1-2 (top), Cases 2-1 and 2-2 (middle), and Cases 2-3 and 2-4 (bottom).

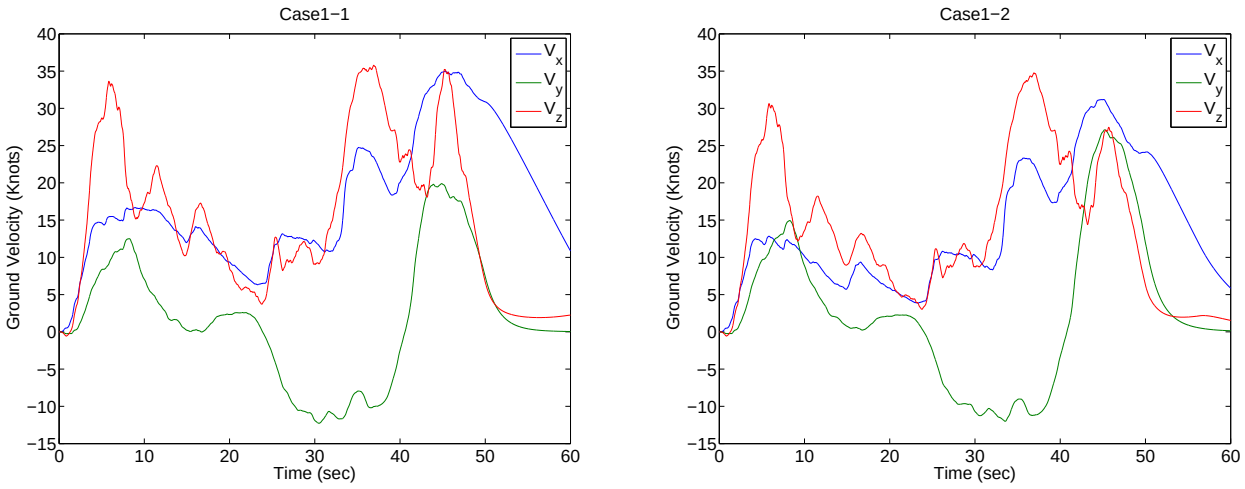

Figure 6: Vehicle ground velocity response while hovering for Cases 1-1 (left) and 1-2 (right).

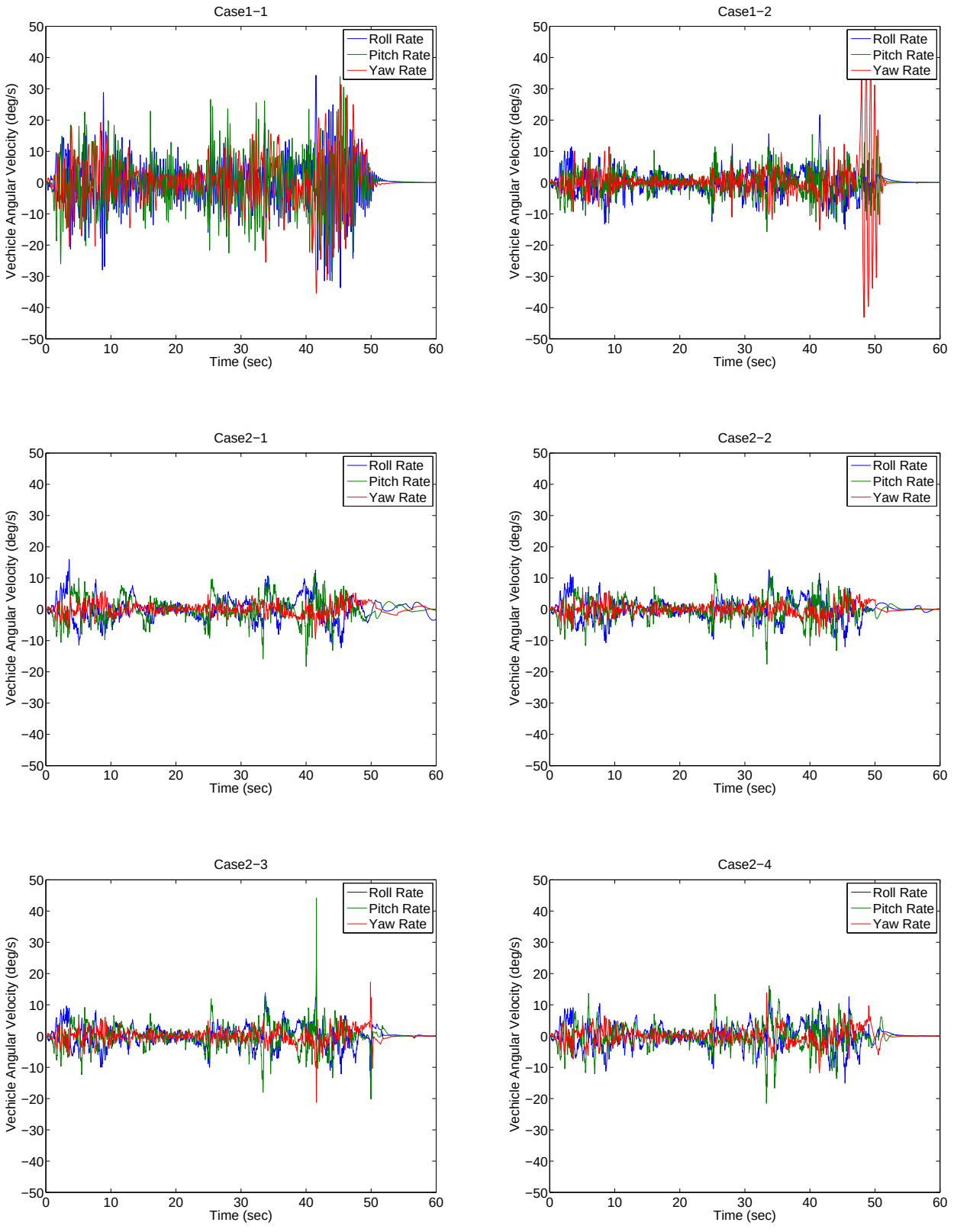

Figure 7: Vehicle angular velocity response to severe air turbulence while hovering for Cases 1-1 and 1-2 (top), Cases 2-1 and 2-2 (middle), and Cases 2-3 and 2-4 (bottom).

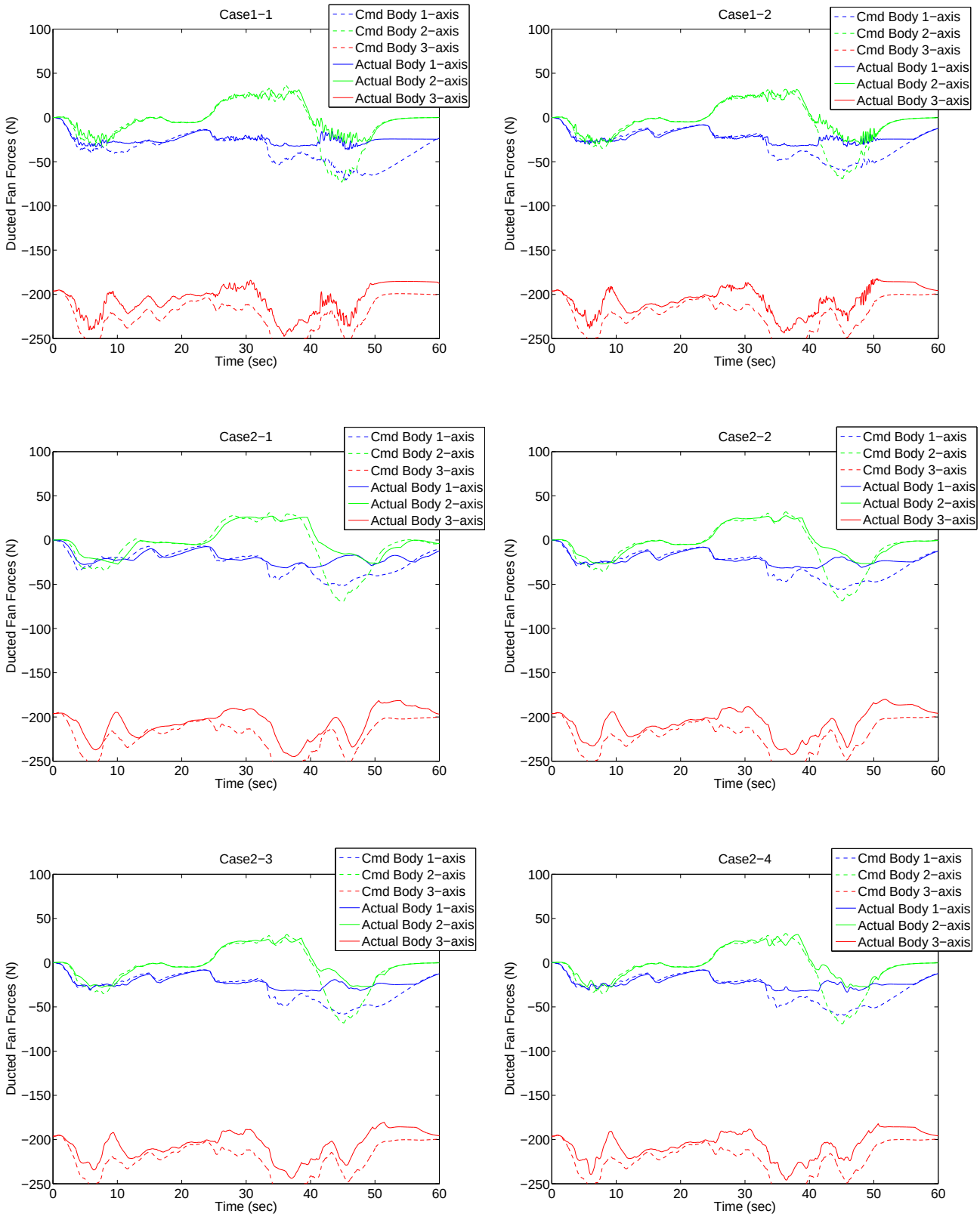

Figure 8: Ducted fan control force responses while hovering for Cases 1-1 and 1-2 (top), Cases 2-1 and 2-2 (middle), and Cases 2-3 and 2-4 (bottom).

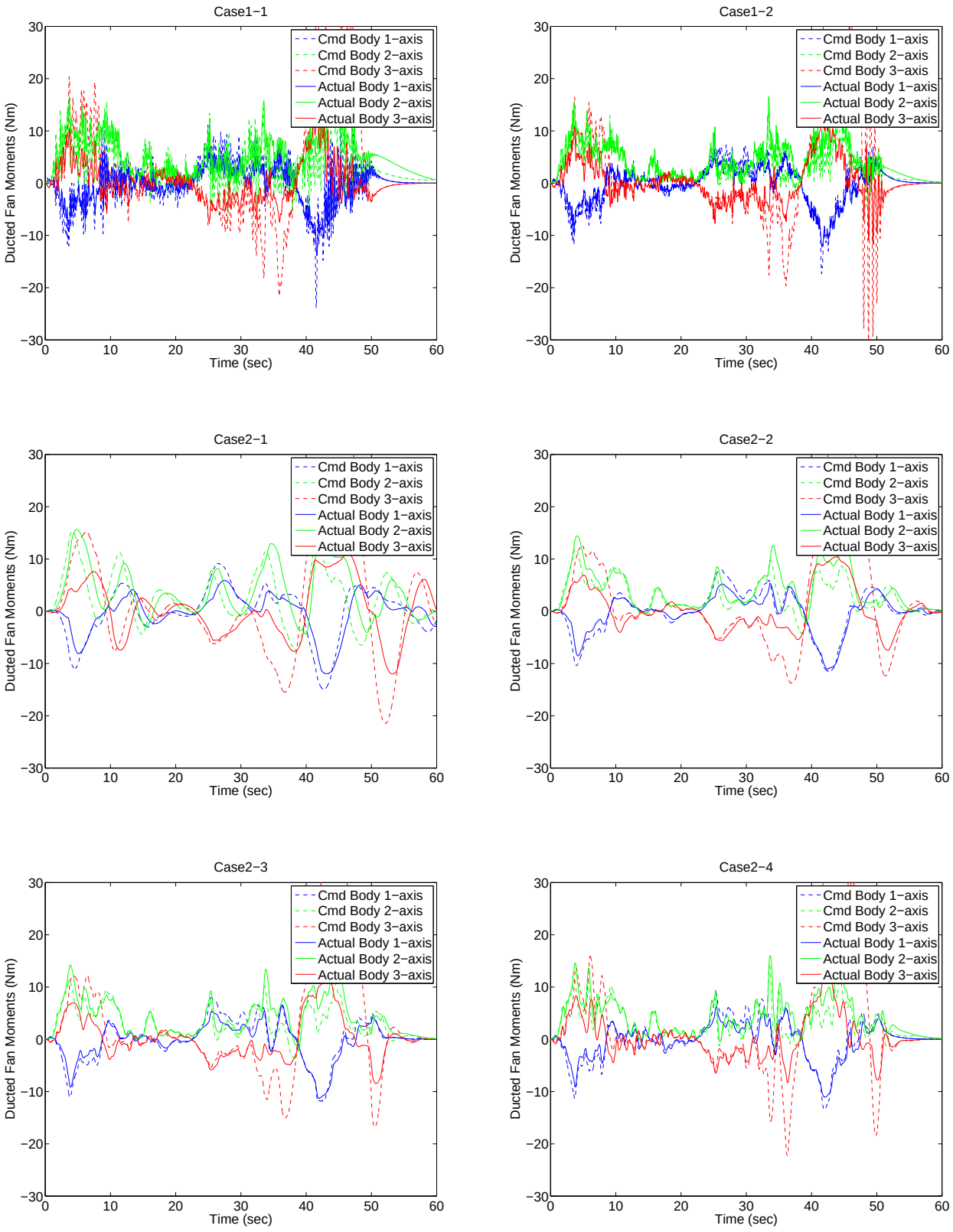

Figure 9: Ducted fan control moment responses while hovering for Cases 1-1 and 1-2 (top), Cases 2-1 and 2-2 (middle), and Cases 2-3 and 2-4 (bottom).

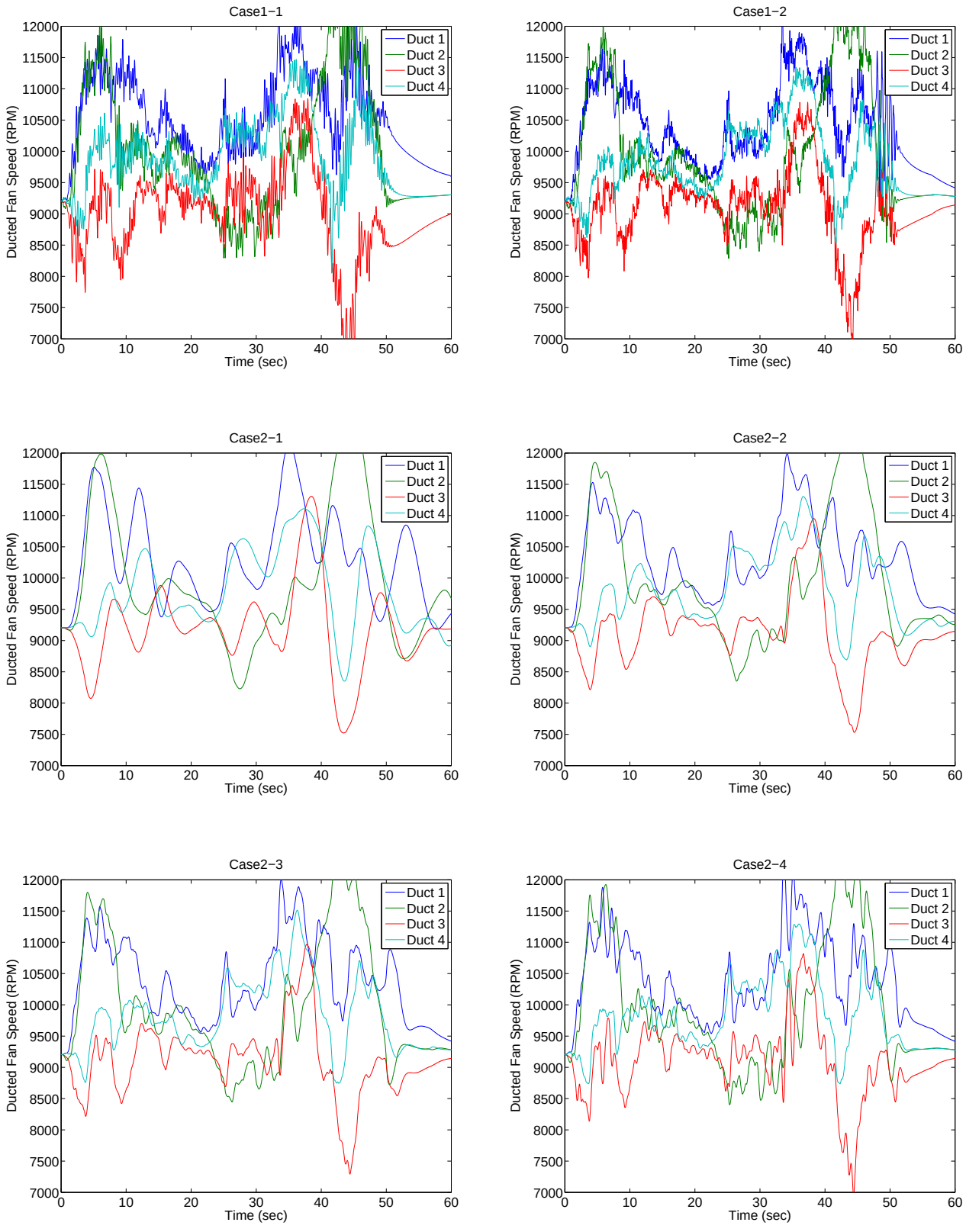

Figure 10: Ducted fan speed responses while hovering for Cases 1-1 and 1-2 (top), Cases 2-1 and 2-2 (middle), and Cases 2-3 and 2-4 (bottom).

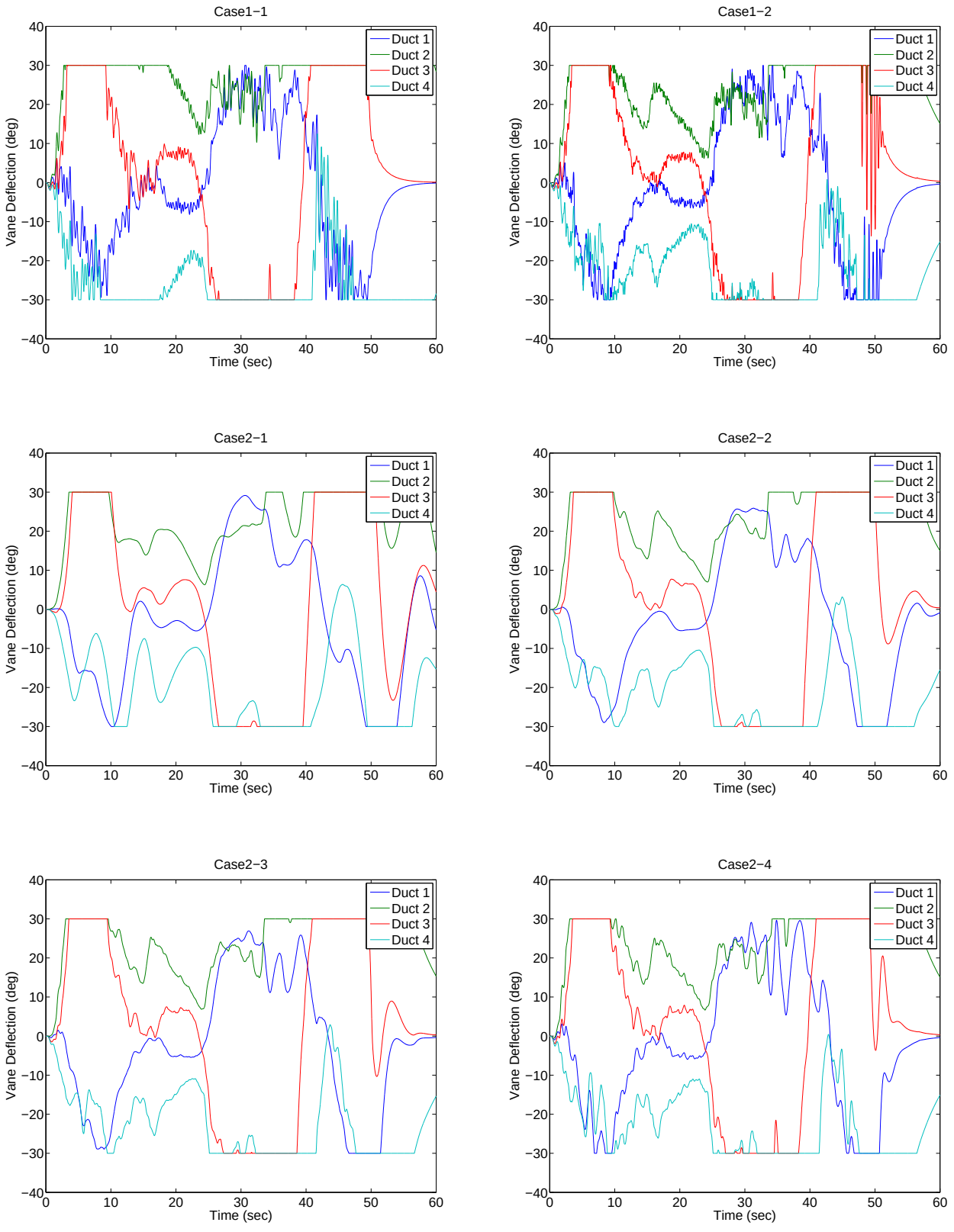

Figure 11: Control vane responses while hovering for Cases 1-1 and 1-2 (top), Cases 2-1 and 2-2 (middle), and Cases 2-3 and 2-4 (bottom).

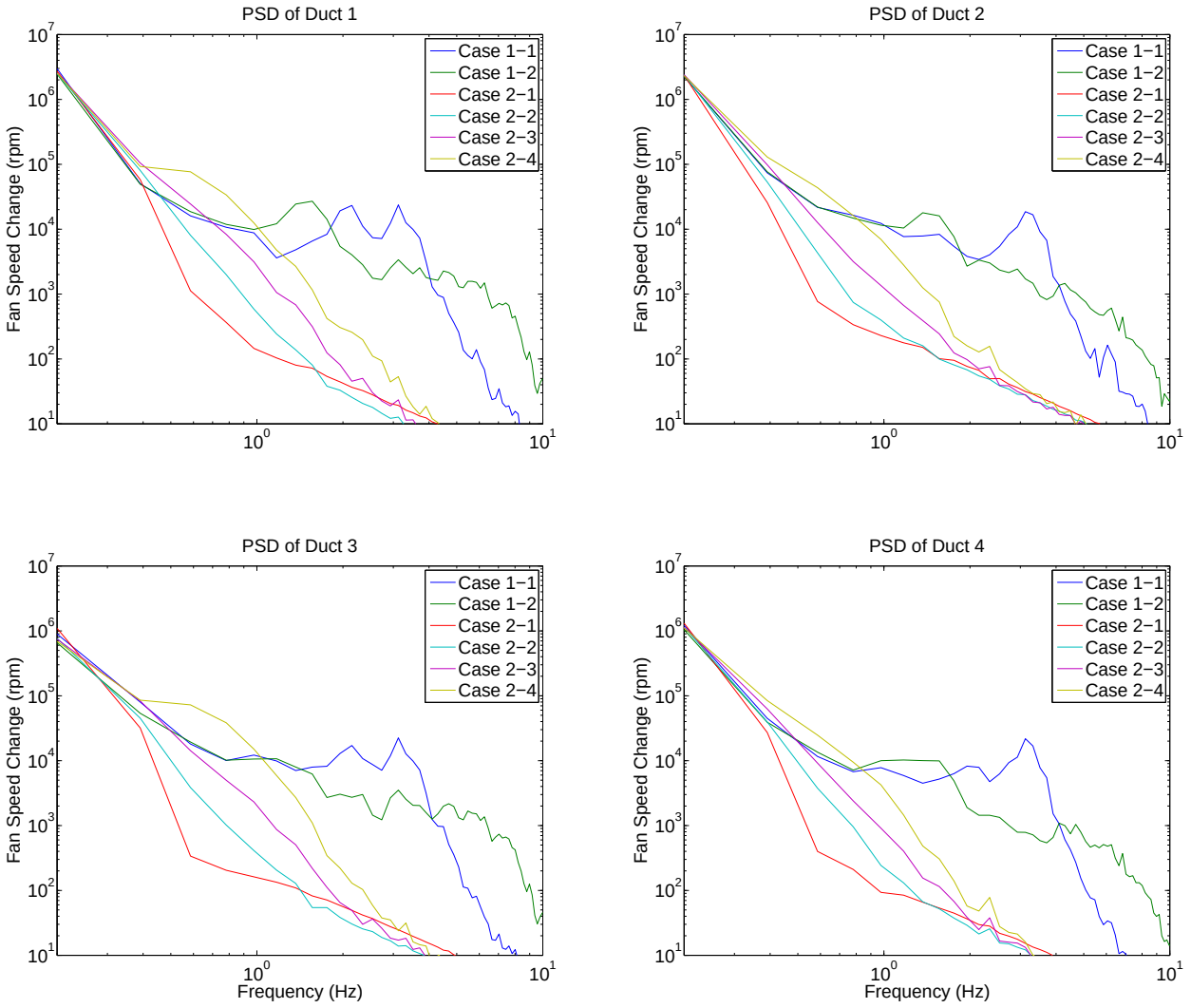

Figure 12: Spectral density of each fan speed response for hovering vehicle under severe turbulence.

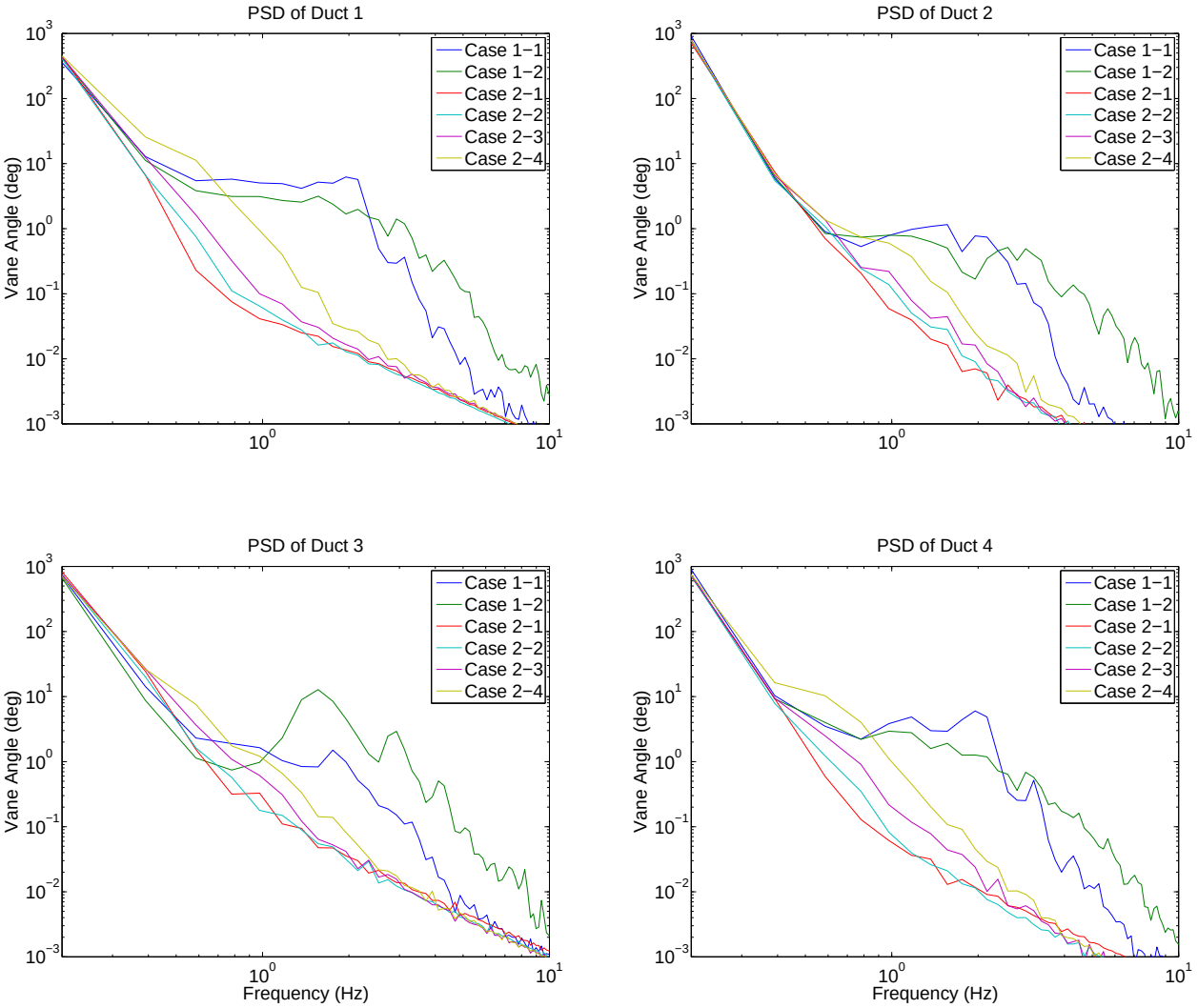

Figure 13: Spectral density of each control vane response for hovering vehicle under severe turbulence.

Case $2-1$

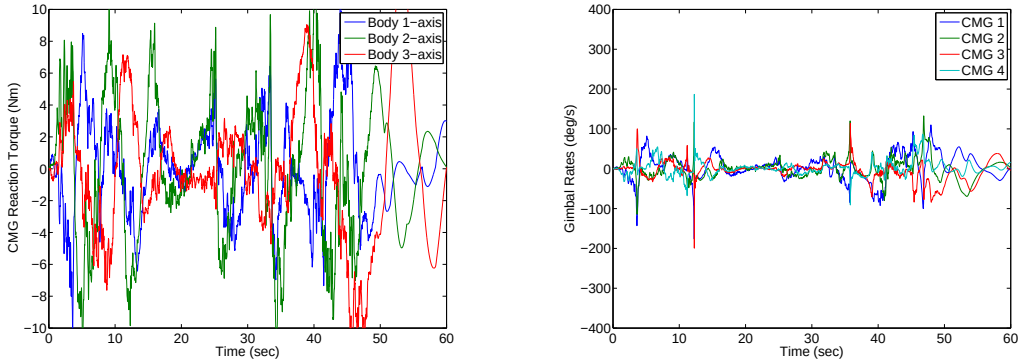

Case $2-2$

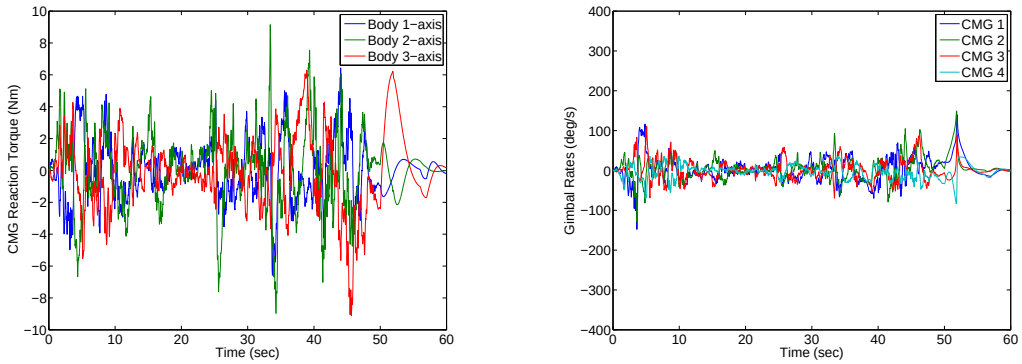

Case $2-3$

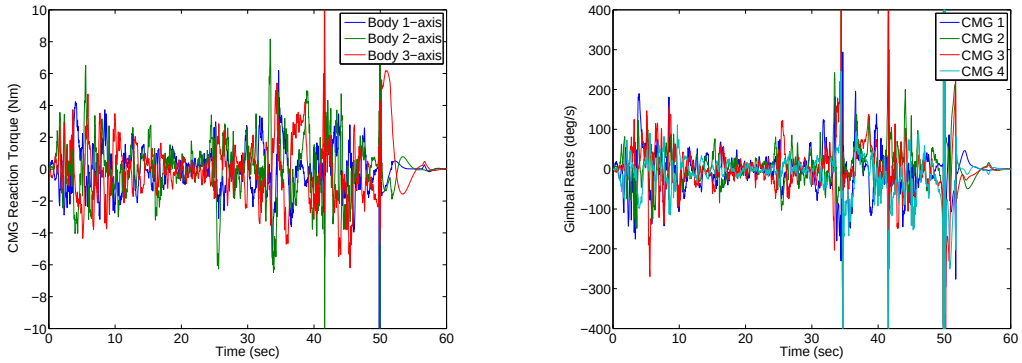

Case $2-4$

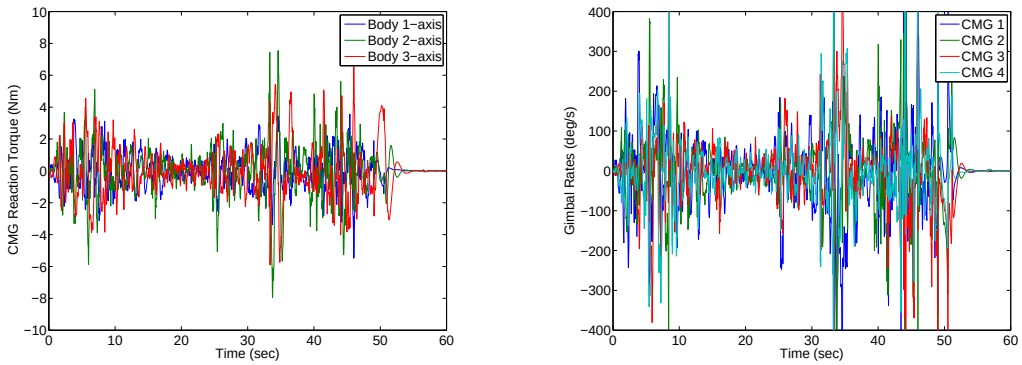

Figure 14: CMG output torque and the corresponding gimbal rate responses while hovering for Case 2-1 (top row), Case 2-2 (second row), Case 2-3 (third row) and Case 2-4 (bottom).

Case $2-1$

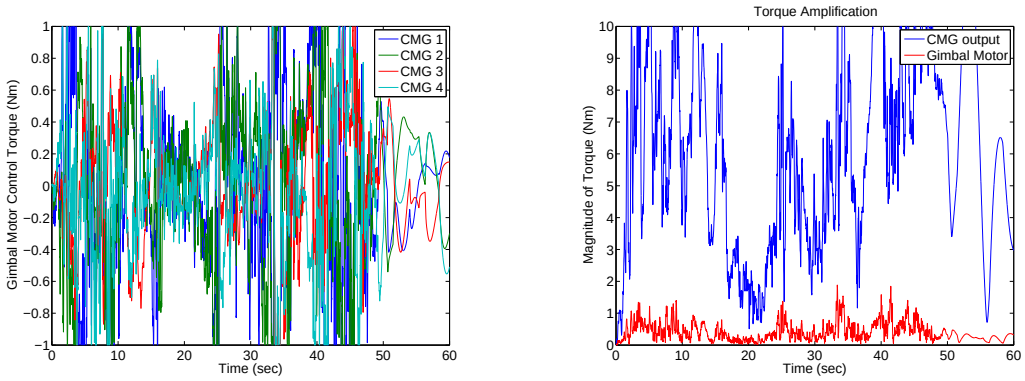

Case $2-2$

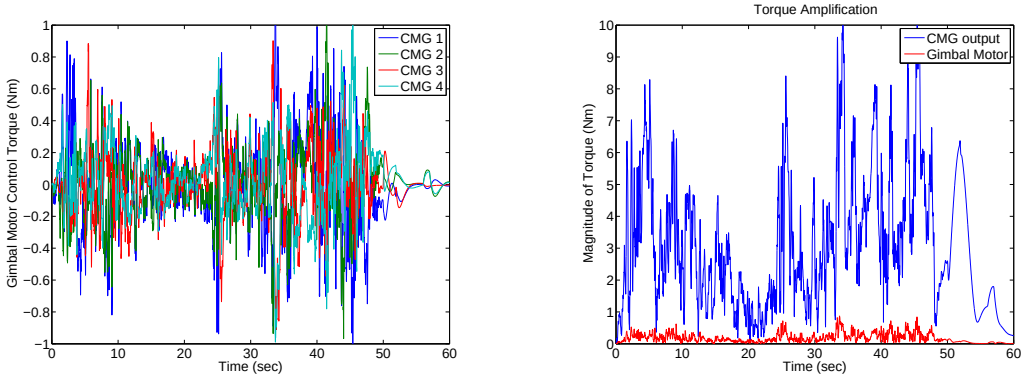

Case $2-3$

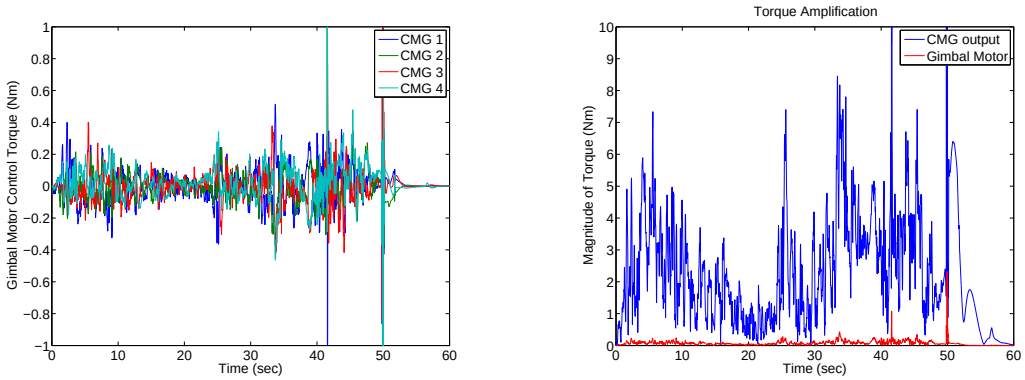

Case $2-4$

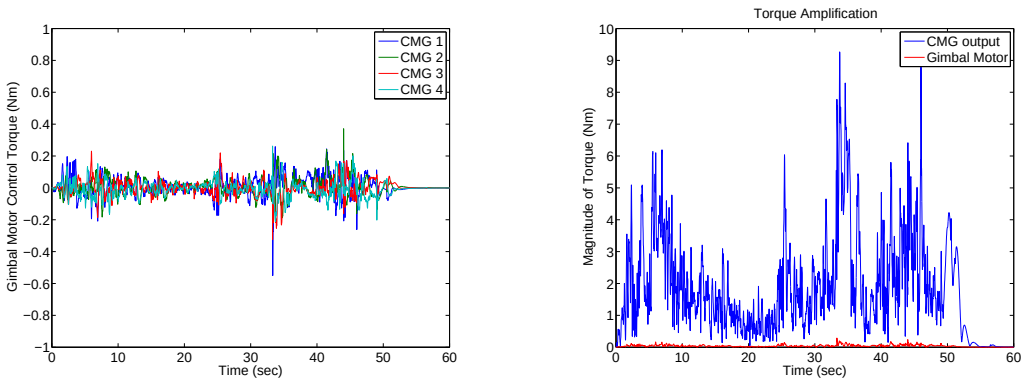

Figure 15: Gimbal motor torque response and the torque amplifications while hovering for Case 2-1 (top row), Case 2-2 (second row), Case 2-3 (third row) and Case 2-4 (bottom).

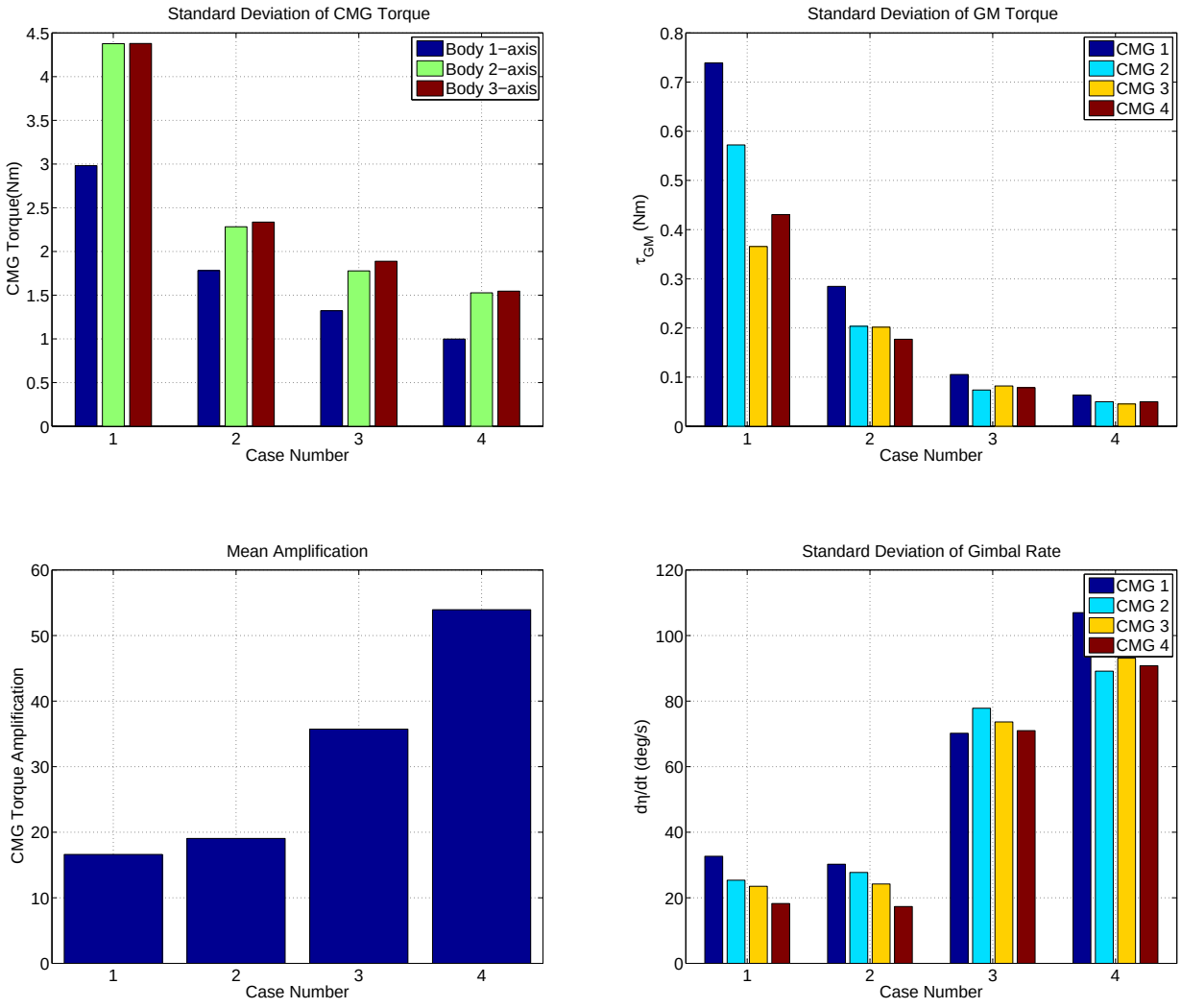

Figure 16: Standard deviation comparions of CMG torques, gimbal motor torques, amplifications, and gimbal rates, for hovering vehicle under severe turbulence for Cases 2-1 to 2-4.

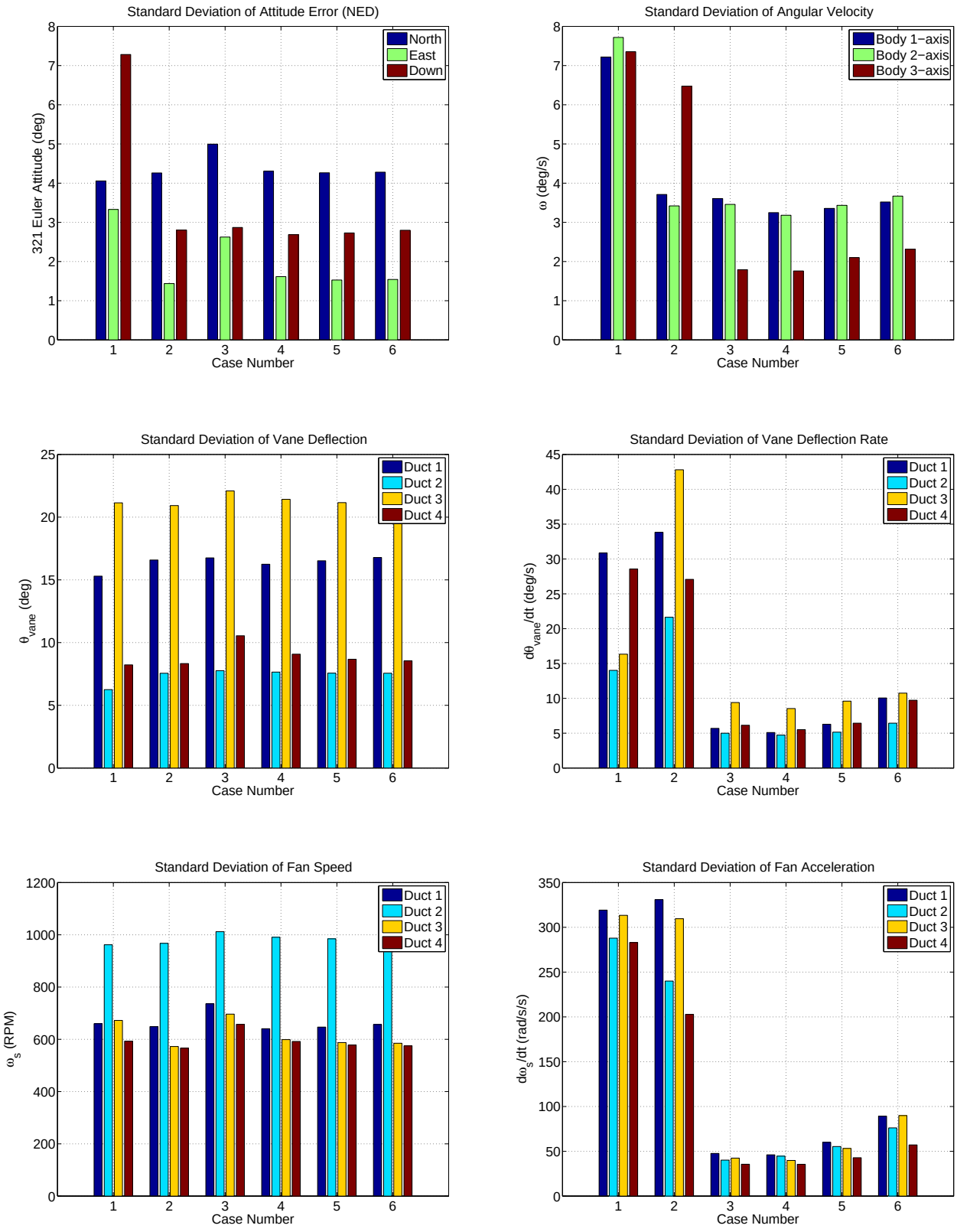

Figure 17: Standard deviation comparions of vehicle attitude and thrust vectoring effector responses.

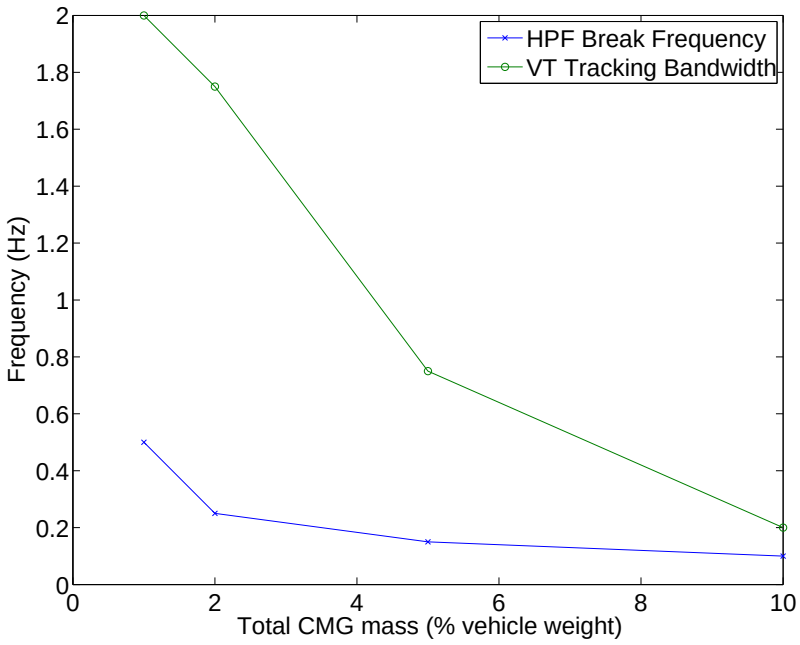

Figure 18: Dependence of high-pass filter break frequency on mass of CMG.